Nigerian Journal of Physics (NJP)
ISSN online: 3027-0936
ISSN print: 1595-0611
Volume 31(1), June 2022

Analysis of Hydromagnetic Stagnation Flow through A Confined Cylinder with A Non-Uniform Heat Source

***[1]Onanuga, O. K., [2]Erusiafe, N. E., [2]Olopade, M. A.**

[1]Department of Applied Physics, Lagos State University of Science and Technology, Ikorodu, Nigeria.
[2]Department of Physics, University of Lagos, Akoka, Lagos State, Nigeria.

*Corresponding Author's Email: onanuga.olutayo@gmail.com Phone: +2348038157341

ABSTRACT

Plasma Physics and magnetohydrodynamics are two branches of study that deal with the motion of electrically conducting fluids (gases and liquids) in a magnetic field. The goal of the study is to analytically improve the existing model of fluid flow behaviour. The flow is governed by a non-dimensional formulated equation. A shooting technique is combined with a fourth-order Runge-Kutta integrated scheme to solve dimensionless momentum and energy equations that satisfy smoothness conditions at the boundary layer's edge. The velocity and temperature distributions are graphically represented with the numerical values for Nusselt number and skin friction and discussed to show the impact of various key embodiment characteristics on the flow. The numerical results were statistically analyzed for the purposes of comparison and correlation and to validate the results of earlier researchers. The developed model numerical results for skin friction coefficient is -0.9694 $\leq f'' \leq$ 4.7293 for stagnation ratio of 0.1 to 3.0 and its Nusselt number is -0.9889 $\leq \theta' \leq$ 1.0702 for power law (n) of-2 to 2. Column statistics revealed a good correlation between the numerical results of the developed model and earlier studies. The Nusselt number mean, standard deviation, and standard error were (2.06, 3.17, and 0.957) as the P values (two tailed) (0.2943, 0.2942). When compared to the previous model, the P value of the developed model indicated an improvement and a good correlation. This research will improve our understanding of the design and construction of a bladeless turbine for microscale electrical power generation using a corotating disc viscous flow generator.

Keywords:
Bladeless,
Dimentionalless,
Magnetohydrodynamic flow,
Thermophysical,
Turbine.

INTRODUCTION

Magnetohydrodynamic (MHD) analysis is concerned with the motion of electrically associated fluids. This principle has been applied in a number of operations, such as flow meters, power generators, pumps, and magnetic medicine treatment. Nonlinear partial differential equations with boundary conditions were transformed into nonlinear ordinary differential equations with the results shown numerically and graphically as fluid flow characteristics. The goal of the study is to analytically improve on the existing model of fluid flow behavior in a stagnation point flow over a permeable surface, which is important for a variety of technical issues, including the development of environmentally friendly stand-alone power generators based on the Tesla bladeless turbine principle.

Magnetohydrodynamic (MHD) analysis is concerned with the motion of electrically accompanied fluids. This principle has been used in a number of operations, such as flow meters, power generators, pumps, and magnetic medicine treatment. The application of appropriate similarity variables is employed to transform nonlinear partial differential equations with boundary conditions into nonlinear ordinary differential equations, with the results shown numerically and graphically as fluid flow characteristics. Chiam (1982) described the properties of the flow and heat transmission of a stretched Newtonian fluid. Sahoo, (2010) reported on a similar type of experiment involving velocity slip and the impact of heat transfer on fluid flow. Hsiao (2011) investigated the drag force induced by permeable wedges and spontaneous convection on non-Newtonian fluids. Nadeem *et al*., (2012) investigated the effect of drag force on Newtonian

fluid motion created by an exponentially stretched sheet. Using an implicit finite-difference technique, Kalteha, *et al*., (2016) numerically derived the semi-similar solution of the Navier–Stokes equations and the energy equation. Bano,*et al*., (2020) analyzed graphically the effects of some governing factors such as curvature parameter, magnetic parameter, wall transpiration parameter, stagnation ratio parameter, and Prandtl number on velocity and temperature profiles. In order to effectively forecast the behavior of an electrically conducting fluid flow, it is necessary to investigate the features of the existing critical thermo-physical parameters included in the model for practical, industrial, and engineering objectives. A mathematical formulation is a one-legged way of communicating a simple active method for estimating the efficiency and performance of a bladeless turbine. This steady flow study was built on the findings of Mastroberardino& Siddique (2014) and Kalteha, *et al*., (2016), who explored heat transfer in MHD stagnation flow through an expanding permeable cylinder. The study did not take into account radiation, viscous dissipation, heat source, or thermal buoyancy, but it did report on the diminishing effect of Reynolds number and magnetic field parameters on flow velocity and temperature profiles.The effect of embedded fluid parameters on the flow momentum and energy balance was investigated by Onanuga, *et al*., (2018) without statistical analysis of the numerical values obtained from the existing model results. For effectively forecasting the behavior of an electrically conducting fluid flow, it is necessary to investigate the features of the existing critical thermo-physical parameters included in the model for experimental purposes.

MATERIALS AND METHODS

The magnetic field's effect on the streamline is assumed to be constant and insignificant. The processes involved are as follows: The mathematical framework for a steady MHD stagnation point within a confined cylinder includes the following: conversion of nonlinear partial differential equations to nonlinear ordinary differential equations via similarity variables; numerical solution using the Shooting technique coupled with the fourth order Runge-Kutta method; and graphical representation of flow behaviour.

Theoretical Framework of the Steady Flow Model

Consider the laminar, hydromagnetic, viscous fluid as well as the two-dimensional boundary layer flow of an electrically conducting, heated, vertical, thin, impermeable, semi-infinite solid cylinder of radius *R*. The cylindrical coordinates (*r, z*) are the axis of the cylinder and are parallel to the uniform composite free stream flow. The origin of the coordinate system is at the center of the leading edge of the cylinder. A uniform magnetic field of strength is applied normally to the flow direction. The cylinder moves linearly with uniform velocity about its axis in the same direction as that of the free stream velocity, and T is the temperature of the fluid. The surface of the cylinder is maintained at a uniform constant temperature while it is at ambient temperature. It is taken as demonstrated in Figure 1. The physical model and coordinate system as well as the equations governing the continuity, momentum, and energy are as follows:

$$\frac{\partial(ru)}{\partial z}+\frac{\partial(rv)}{\partial r}=0 \quad (1)$$

$$u\frac{\partial u}{\partial z}+v\frac{\partial u}{\partial r}=-\frac{1}{\rho}\frac{dP_e}{dz}+\frac{\nu}{r}\frac{\partial}{\partial r}\left(r\frac{\partial u}{\partial r}\right)-\frac{\sigma B_0^2 u}{\rho}+g\beta(T-T_\infty)-\frac{\nu}{k_0}u \quad (2)$$

$$u\frac{\partial T}{\partial z}+v\frac{\partial T}{\partial r}=\frac{k}{\rho c_p}\frac{1}{r}\frac{\partial}{\partial r}\left(r\frac{\partial T}{\partial r}\right)-\frac{1}{\rho c_p}\frac{1}{r}\frac{\partial}{\partial r}(rq_0)+\frac{\nu}{c_p}\left(\frac{\partial u}{\partial r}\right)^2+\frac{q'''}{\rho c_p} \quad (3)$$

Subject to no-slip boundary conditions

$$u(r,z)=U_w(\mathrm{r},\mathrm{z})=\frac{u_0 z}{l}, v(r,\mathrm{z})=-v_w,$$
$$T(\mathrm{r},\mathrm{z})=T_w(r,z)=T_\infty+\left(\frac{z}{l}\right)^n\Delta T \ at \ r=0$$
$$u(\mathrm{r},\mathrm{z})=u_e(r,z)=\frac{u_\infty z}{l}, T(\mathrm{r},\mathrm{z})=T_\infty \ as \ r\longrightarrow\infty \quad (4)$$

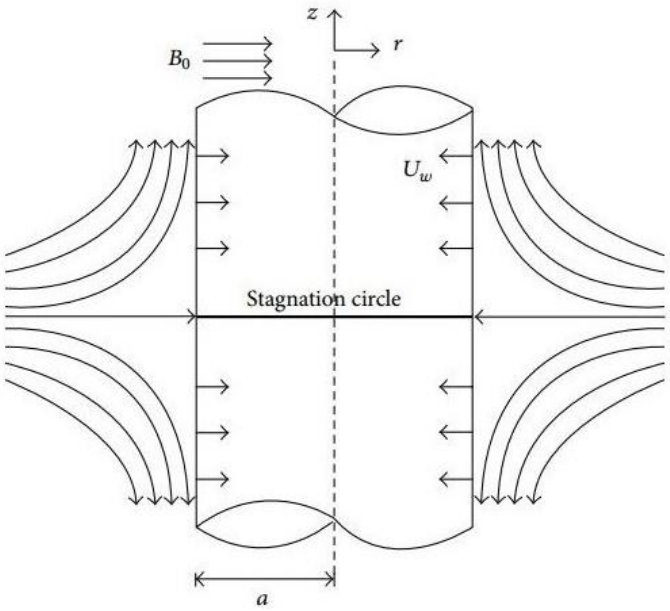

Figure 1: The Schematic Steady Flow Model Of (Kalteha , Ghorbania, & Khademinejadb, 2016)

From the above, $\boldsymbol{u}$ and $\boldsymbol{v}$ are the velocity components in the z and r directions respectively. Also the parameters $P_e, \nu, \rho, \sigma, B_0, g, \beta,$ and k_o are respectively the stretching pressure, kinematic viscosity, fluid density, electrical conductivity, uniform magnetic field, the acceleration due to gravity, the coefficient of expansivity, and porous permeability parameter. k, c_p, q_0, u_0 and u_∞ are the thermal conductivity, specific heat at constant pressure, thermal radiation, stretching velocity and free stream velocity, respectively.

The term $\frac{dP_e}{dz}$ in equation (2) can be defined as

$$\frac{dP_e}{dz} = -\rho u_e \frac{du_e}{dz} - \sigma B_o^2 u_e$$

While the radiation term in equation (3) is defined as

$$q_o = -\frac{16\sigma_0 T_\infty^3}{3\delta}\frac{\partial T}{\partial r}$$

And the non-uniform heat source/sink is expressed as

$$q''' = \frac{ku_o(z)}{lv}[\lambda(T - T_\infty) + \lambda^*(T_w - T_\infty)e^{-\eta}].$$

The similarity variables is expressed in equation (5) as

$$\text{u}= \frac{u_o z}{l}f'(\eta),\ \upsilon = -\frac{a}{r}\left(\frac{u_o \upsilon}{l}\right)^{\frac{1}{2}}f(\eta), \theta(\eta) = \frac{T-T_\infty}{T_w - T_\infty}\ ,\psi = \left(\frac{\upsilon u_o}{l}\right)^{\frac{1}{2}}$$

$$\text{za}f(\eta), \eta = \left(\frac{r^2 - a^2}{2a}\right)\left(\frac{u_o}{\upsilon l}\right)^{\frac{1}{2}}$$

$$\frac{\partial u}{\partial z} = \frac{u_o}{l}f'(\eta);\ \frac{\partial v}{\partial r} = \frac{1}{r^2}\left(\frac{\upsilon u_o}{l}\right)^{\frac{1}{2}}af(\eta) - \frac{1}{r}\left(\frac{\upsilon u_o}{l}\right)^{\frac{1}{2}}\text{a}f'(\eta)\frac{\partial \eta}{\partial r}\ ;\ \frac{\partial \psi}{\partial r} = \frac{u_o r z}{l}f'(\eta) \quad (5)$$

$$\frac{\partial \psi}{\partial z} = \left(\frac{\upsilon u_o}{l}\right)^{\frac{1}{2}}\text{a}f(\eta); \frac{\partial \eta}{\partial r} = \frac{r}{a}\left(\frac{u_o}{\upsilon l}\right)^{\frac{1}{2}}\ ;\ \frac{\partial \eta}{\partial z} = 0;$$

Stream function is expressed as

$$\text{u} = \frac{1}{r}\frac{\partial \psi}{\partial r};\ \text{v} = -\frac{1}{r}\frac{\partial \psi}{\partial r} \quad (6)$$

Substitute Equations (5) and (6) into Equation (1) we have

$$\frac{u_o}{l}f'(\eta) + \frac{1}{r^2}\left(\frac{\upsilon u_o}{l}\right)^{\frac{1}{2}}af(\eta) - \frac{1}{r}\left(\frac{\upsilon u_o}{l}\right)^{\frac{1}{2}}\text{a}f'(\eta)\frac{r}{a}\left(\left(\frac{u_o}{\upsilon l}\right)^{\frac{1}{2}}\right) - \frac{a}{r^2}\left(\frac{u_o \upsilon}{l}\right)^{\frac{1}{2}}f(\eta) = 0$$

$$\frac{u_o}{l}f'(\eta) + \frac{a}{r^2}\left(\frac{\upsilon u_o}{l}\right)^{\frac{1}{2}}f(\eta) - \frac{1}{r}\left(\frac{\upsilon u_o}{l}\right)^{\frac{1}{2}}\text{a}f'(\eta)\frac{r}{a}\left(\left(\frac{u_o}{\upsilon l}\right)^{\frac{1}{2}}\right) - \frac{a}{r^2}\left(\frac{u_o \upsilon}{l}\right)^{\frac{1}{2}}f(\eta) = 0$$

$$\frac{u_o}{l}f'(\eta) + \frac{a}{r^2}\left(\frac{\upsilon u_o}{l}\right)^{\frac{1}{2}}f(\eta) - \frac{u_o}{l}f'(\eta) - \frac{a}{r^2}\left(\frac{u_o \upsilon}{l}\right)^{\frac{1}{2}}f(\eta) = 0$$

$$\frac{u_o}{l}f'(\eta) - \frac{u_o}{l}f'(\eta) = 0 \quad (7)$$

The continuity equation (1) is satisfied as shown in equation (7).

Applying the similarity variables in equations (5) and (6) to the main governing equations (2) to (4), the governing equations and the boundary conditions are transformed into nonlinear coupled ordinary differential equations, with the appropriate non-dimensional similarity variables as follows, to give equations (8), (9), and (10).

$$(1 + 2K\eta)f'''(\eta) + 2Kf''(\eta) + f(\eta)f''(\eta) - (f'(\eta))^2 - H^2(f'(\eta) - \gamma) - f'(\eta)(\text{Z} - \gamma) + Gr\theta(\eta) = 0, \quad (8)$$

$$\left(1 + \frac{4}{3}N\right)((1 + 2K\eta)\theta''(\eta) + 2K\theta'(\eta)) + Prf(\eta)\theta'(\eta) - nPrf'(\eta)\theta(\eta) + \lambda^* e^{-\eta} + \lambda\theta + EcPr(1 + 2K\eta)(f''(\eta))^2 = 0 \quad (9)$$

Subject to the boundary conditions,

$$f'(\eta) = 1, f = f_w, \theta = 1, at\ \eta = 0,\quad f' = \gamma,\ \theta = 0, as\ \eta \to \infty \quad (10)$$

where $K = \frac{1}{a}\sqrt{\frac{l\nu}{u_0}}$ is the curvature parameter, $Z = \frac{\upsilon l}{k_o u_o}$ is the permeability parameter, $H^2 = \frac{\sigma B_0^2 l}{\rho u_0}$ is the Hartman number, $Gr = \frac{l^2 g\beta(T_w - T_\infty)}{zu_0^2}$ is the thermal Grashof number, $\gamma = \frac{u_e}{U_w}$ is the stagnation rate ratio $N = \frac{4\sigma_0 T_\infty^3}{\delta k}$ is the radiation parameter,

$P_r = \frac{\mu C_p}{k}$ is the Prandtl number, $Ec = \frac{u_0^2}{C_p(T_w - T_\infty)}$ is the Echert number, $f_w = v_w\sqrt{\frac{a}{\nu u_0}}$ is the suction $f_w > 0$ or injection $f_w < 0$ parameter.

The engineering quantities of interest are the skin friction (C_f) and Nusselt number (Nu) defined as follows

$$C_{fz} = \frac{2\tau_w}{\rho u_0^2}, \Longrightarrow R_{ez}^{\frac{1}{2}} C_{fz} = f''(0) \quad (11)$$

$$N_{uz} = \frac{zq_w}{k(T_w - T_\infty)}, \Longrightarrow R_{ez}^{-\frac{1}{2}} N_{uz} = -\left(1 + \frac{4}{3}N\right)\theta'(0) \quad (12)$$

Where

$$\tau_w = \mu\left(\frac{\partial u}{\partial r}\right)_{r=R} = \left(\frac{\partial u}{\partial r} + \left(\nu\,\frac{\partial^2 u}{\partial r^2} + \frac{\partial^2 u}{\partial z \partial r}\right)\right)_{r=R} \text{ and}$$

$$q_w = -k\left(\frac{\partial T}{\partial r}\right)_{r=R} = -\left(k + \frac{16\sigma_0 T_\infty^3}{3\delta}\right)\left(\frac{\partial T}{\partial r}\right)_{r=R} \quad (13)$$

are defined and $R_{ez} = \frac{zu_0}{\nu}$ shows the local Reynolds number.

Here, the fourth-order Runge-Kutta method is applied to solve the equation (8) to (10), and the scheme for fourth-order Runge-Kutta as

$$y_{n+1} = y_n + \frac{h}{6}(k_1 + 2k_2 + 2k_3 + k_4) \quad (14)$$

Where;

$k_1 = f(x_n, y_n),$

$k_2 = f\left(x_n + \frac{h}{2}, y_n + \frac{hk}{2}\right),$

$k_3 = f\left(x_n + \frac{h}{2}, y_n + h\frac{k_2}{2}\right),$

$k_4 = f(x_n + h, y_n + hk_3),$

The method has been proven to be adequate for boundary layer equations. It is seen to give accurate results, and has been widely used. The scheme is also applicable to various types of boundary layer flow problems, including free and mixed convection flows. The problem is a boundary value problem with the application of a shooting technique (guessing the unknown values) to change the conditions of the initial value problem.

Let,

$$\begin{bmatrix} x_1 \\ x_2 \\ x_3 \\ x_4 \\ x_5 \\ x_6 \\ x_7 \end{bmatrix} = \begin{bmatrix} \eta \\ f \\ f' \\ f'' \\ f''' \\ \theta \\ \theta' \end{bmatrix} \quad (15)$$

Then, it becomes,

$$\begin{bmatrix} x'_1 \\ x'_2 \\ x'_3 \\ x'_4 \\ x'_5 \\ x'_6 \\ x'_7 \end{bmatrix} = \begin{bmatrix} 1 \\ x_3 \\ x_4 \\ x_5 \\ \frac{-2kx_{4-x_2x_4+(1+Z)x_3^2-H^2(x_3+\gamma)-\gamma^2-Grx_6}}{1+2kx_1} \\ x_6 \\ \frac{-2kx_7-Prx_2x_7+nPrx_3x_6-\lambda^* e^{-x_1}-\lambda x_6-EcPr(1+2kx_1)x_4^2}{(1+\frac{4}{3})(1+2kx_1)} \end{bmatrix} \quad (16)$$

$$\begin{bmatrix} x_{1(0)} \\ x_2(0) \\ x_{3(0)} \\ x_{4(0)} \\ x_{5(0)} \\ x_{6(0)} \\ x_{7(0)} \end{bmatrix} = \begin{bmatrix} 0 \\ f_w \\ 1 \\ a_1 \\ \gamma \\ a_2 \\ a_3 \end{bmatrix} \quad (17)$$

Where $f_w, \gamma, a_1, a_2, a_3$ are unknown constants to be determined?

The computations have been performed using a mathetica symbolic program on MAPLE 2016. The step size is taken to be $\Delta\eta = 0.001$ to satisfy the convergence requirement of 10^{-5} in all cases. The value of η_∞ is noticed to the iteration loop by $\eta_\infty = \eta_\infty + \Delta\eta$ The highest value of η_∞ in each parameter is determined when the values of the unknown boundary conditions at $\eta = 0$ did not change to a successful loop with an error less than 10^{-5}.

RESULTS AND DISCUSSION

Results of the Steady Flow Model

The numerical values of the steady flow for local skin friction coefficient $f''(0)$ and Nusselt number $\theta'(0)$ arepresented in Tables 4 and 5respectively.

Table 4: Comparison Of Numerical Values Of The Steady Flow For $f''(0)$ When $K = 0, H = 0, Gr = 0, Z = 0, \lambda = 0, n = 0, \lambda^* = 0, N = 0, f_w = 0, Pr = 1, Ec = 0.2, \eta \longrightarrow \infty$

γ	(Pop, Grosan, & Pop, 2004)	(Sharma & Singh, 2009)	(Hayat, Qayyam, & Alsaedi, 2014)	Present results
0.1	-0.9694	-0.969386	-0.9679	-0.9694
0.2	-0.9181	-0.9181069	-0.9172	-0.9181
0.5	-0.6673	-0.667263	-0.6670	-0.6673
2.0	2.0174	2.01749079	2.0174	2.0174
3.0	4.7293	4.72922695	4.7294	4.7293

Table 5: Comparison Of Numerical Values Of The Steady Flow For $\theta'(0)$ When $K = 0, H = 0, Gr = 0, Z = 0, \gamma = 0, \lambda = 0, \lambda^* = 0, N = 0, f_w = 0, Pr = 1, Ec = 0.2, \eta \longrightarrow \infty$

Pr	n	(Mukhopadhyay, 2012)	(Pal & Mondal, 2012)	(Hayat, Qayyam, & Alsaedi, 2014)	Present results
1	-2	-	-	-1.0000	-0.9889
	-1	-	-	-0.0	-0.0025
	0	-0.5821	-	-0.5832	-0.5826
	1	1.0000	-	1.0000	1.0002
	2	1.3332	1.333333	1.3332	1.3333
10	-2	-	-	10.0000	9.9964
	-1	-	-	0.0	0.0
	0	-	-	2.3080	2.3080
	1	-	-	3.7207	3.7206
	2	-	4.796871	4.7969	4.7968
0.7	2	-	-	1.0791	1.0702
0.6	2	-	-	-	0.9708
0.5	2	-	-	-	0.8637

The numerical values obtained for the coefficient of skin friction $f''(0)$ of the steady flow as compared with the statistical analysis reveal a strong correlation between the study and the results from Hayat, *et al*., (2014). Both have negligible P values of 0.0886 with the same values for mean 0.839, standard error 1.12, and standard deviation 2.51 and a 95% confidential interval of 0.8707 to 0.9995 of Table 4. Table 5 compares the present numerical values for the Nusselt number $\theta''(0)$ of the steady flow model with previous work and statistical analysis established a good correlation and agreed with previous findings. Hayat *et al*. (2014) had a P value of 0.2943 and the developed model had a P value of 0.2942, implying a better of the same mean 2.06, standard error 0.957, and standard deviation 3.17 with a 95% confidential interval of discrepancy – 1.07 to 3.19 for both. The graphical interpretations of the thermophysical parameters of the steady flow model are shown in Figure 7 (a-e).

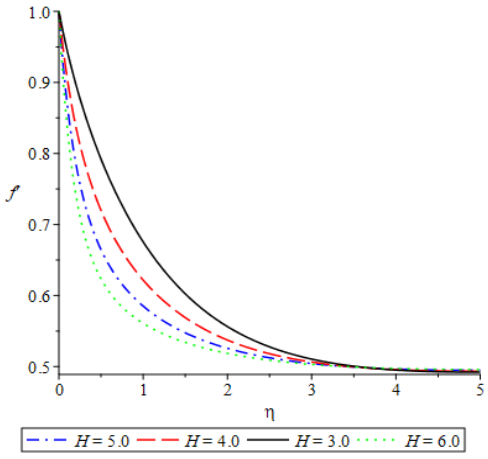

Figure 7a: velocity profile for different values of H(Hartmann)

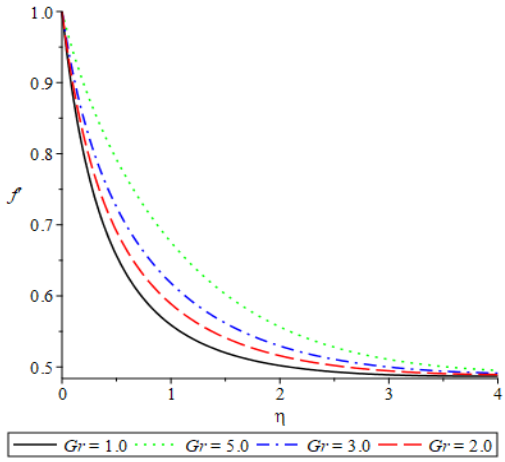

Figure 7b: velocity profile for different values of Grashof

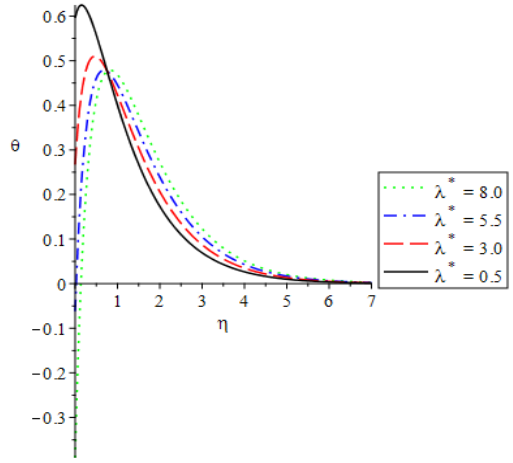

Figure 7c: Temperature profile for different values of λ^*

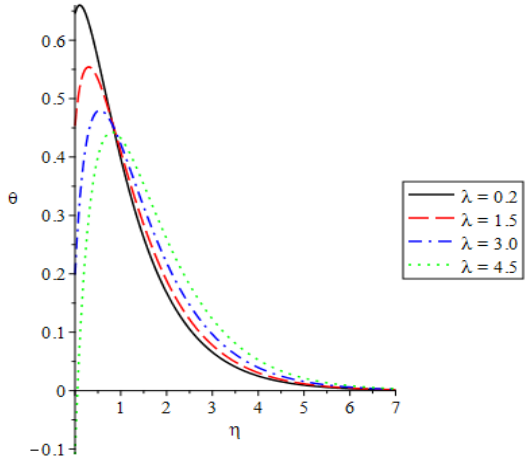

Figure 7d: Temperature profile for different values of λ

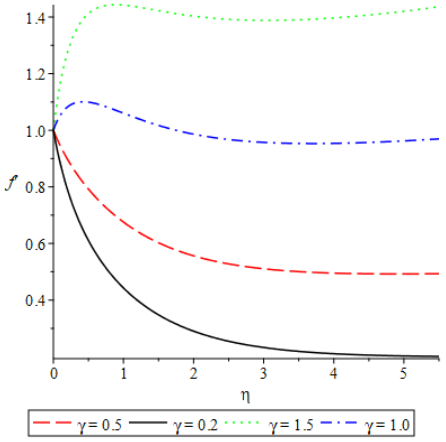

Figure 7e: velocity profile for different values of γ (stagnation rate)

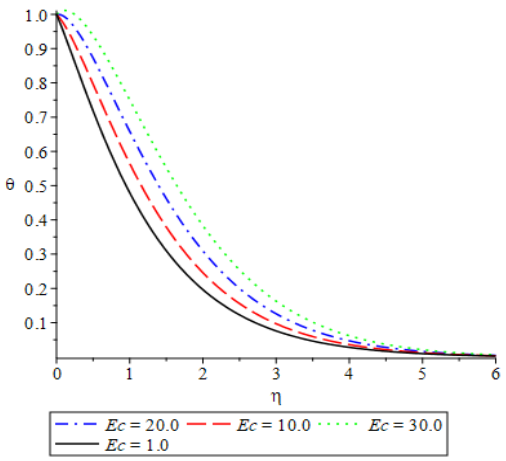

Figure 7f: Temperature profile for different values of Ec (Eckert number)

The nonlinear differential equations (8) to (10) and their boundary conditions are numerically solved using the shooting approach in conjunction with the fourth order Runge-Kutta integration algorithm method. Except otherwise stated on the respective graphs, calculations are performed using various values of the following default parameters: Pr = 0.72, H = 3.0, Gr = 5.0, K = 2.0, N = 1.0, Ec = 0.5, Z = 1.0, and fw = 0.5, and the smoothness conditions at the boundary layer are satisfied.

The effect of different magnetic field parameter H values on the velocity profile is shown in Figure 7(a).The pace of fluid motion is shown to be significantly slowed as the H values increase. The Lorentz force induced by the magnetic field causes the damping magnetic parameters to increase.

The effect of different thermal Grashof number (Gr) values on the velocity profile is shown in Figure 7 (b). Gr denotes the ratio of thermal buoyancy to viscous hydrodynamic force. For the effects of thermal buoyancy, increasing the value of Gr improves flow in the boundary layer.

Figures 7(c) and 7(d) depict the effect of a variational increase in the values of non-uniform heat generating parameters on heat distribution near the surface, which is observed as a decrease but later increases. It can be seen that as the non-uniform heat generating parameters are increased, the boundary layer thickness also increases, increasing the speed of the fluid in the system. Figure 7 (e) shows the effect of varying the stagnation ratio parameter on the dimensionless velocity profile. Because the stretching velocity is greater than free stream flow, the boundary layer thickness increases for values greater than 0, and hence the velocity profile increases. Thermal boundary layer thickness decreases as heat is rejected, resulting in a decrease in temperature profile. The influence of the viscous dissipation parameter Ec on the energy gradient is depicted in Figure 7(f). The Eckert number is the ratio of the flow's kinetic energy to the

difference in boundary layer enthalpy. Works done against viscous fluid strains convert kinetic energy to internal energy. Increases in the Ec parameter increase the energy at any point in the f low, causing the temperature profile to change.

CONCLUSION

The study revealed that the developed model was better with 95% confidence interval for Nusselt number ranged from 0.6381 to 0.5590 than 95% confidence interval of Hayat *et al* (2014) that ranged from – 0.6377 to 0.5594. It provided significantly faster searches with sufficient accuracy for skin friction coefficient and Nusselt number of the past to present work.

The analysis of the developed model with incorporated thermophysical parameters produced numerical results for skin friction coefficient that ranged from -0.9694 ≤ $f'' \leq$ 4.7293 for stagnation ratio ranging from 0.1 to 3.0 and its Nusselt number ranged from -0.9889 ≤ $\theta' \leq$ 1.0702 for power law (n) ranging from-2 to 2. Column statistics revealed a good correlation between the numerical results of the developed model and earlier studies. The Nusselt number mean, standard deviation, and standard error were (2.06, 3.17, and 0.957) as the P values (two tailed) (0.2943, 0.2942). When compared to Hayat, Qayyam, &Alsaedi (2014), the P value of the developed model indicated an improvement and a good correlation. The modified model's graphical depiction revealed that as the Hartman number increases within the system, velocity decreases as temperature increases, and the temperature profile and boundary layer thickness increase as the Eckert number increases. It provided significantly faster searches with sufficient accuracy for skin friction coefficient and Nusselt number of the past to present work.

REFERENCES

Bano, N., Singh, B. B., & Sayyed, S. R. (2020). MHD Stagnation Point Flow and Heat Transfer over an Exponentially Stretching/Shrinking Vertical Permeable Cylinder. Diffusion Foundations, 26, 23-38.

Chiam, T. C. (1982). Heat transfer in a fluid with variable thermal conductivity over a linearly stretching sheet. Journal of engineering science 20, 6, 737-745.

Hayat, T., Qayyam, S., & Alsaedi, A. (2014). Effects of heat and mass transfer in flow along avertical stretching cylinder with slip conditions. Eup. Phys.J.Plus 129:63.

Hsiao, K. L. (2011). .MHD mixed convection for viscoelastic fuid past a porous wedge. International Journal Nonlinear Mech 46, 1–8.

Kalteha, M., Ghorbania, S., & Khademinejadb, T. (2016). Viscous dissipation and thermal radiation effects on the magnetohydrodynamic (MHD) flow and heat transfer over a stretchingslender cylinder. Journal of Applied Mechanics and Technical Physics, 57(3), 463-472.

Mastroberardino, A., & Siddique. (2014). Magnetohydrodynamic stagnation flow and heat transfer toward a stretching permeable cylinder. Hindawi Publishing Corporation Advances in Mechanical Engineering Volume 2014, Article ID 419568, 5.

Mukhopadhyay, S. (2012). Mixed convection boundary layer flow along a stretching cylinder in porous medium. Journal Applied Math, 73-78. Journal Applied Math, 73-78.

Nadeem , S., Rehman, A., Lee , C., & Lee, J. (2012). Boundary layer flow of second grade fluid in a cylinder with heat transfer. Journal: Mathematical problems in engineering, Doi.10.1155/2012/640289.

Onanuga, O. K., Chendo, M. A., & Erusiafe, N. E. (2018). Thermal Radiation of Hydromagnetic Stagnation Gravity-Driven Flow through a Porous Confined Cylinder with Non-Uniform heat source. Scientific research publishing, 1 - 17.

Pal, D., & Mondal, H. (2012). Hydromagnetic convective diffusion of species in Darcy-Forchheimer porous medium with non-uniform heat source/sink and variable viscosity. Elsevier Journal, volume 39, Issue 7, 913 – 917.

Pandey, R. J., Pudasaini, S., Dhakal, S., Uprety, R. B., & Neopane, H. P. (2014). Design and computational analysis of 1 kW Tesla turbine. International Journal of scientific and research publications, 4(9), 1-4.

Pop, S. R., Grosan, T., & Pop, I. (2004). Radiation effect on the flow near the stagnation point of a stretching sheet. Tech. Mechanic 25, 100 - 106.

Sahoo, B. (2010). Flow and heat transfer of a non-Newtonian fuid past a stretching sheet with partial slip. Commun Nonlinear Sci Numer Simul 15, 602–615.

Sharma, P. R., & Singh. (2009). Effects of variable thermal conductivity and heat source/sink onMHD flow near a stagnation point on a linearly stretching sheet. Journal.Applied fluid mechanics, 2, 13-21.